RSC Advances

PAPER

View Article Online
View Journal | View Issue

Cite this: *RSC Adv.*, 2026, **16**, 26609

Improving catalytic aquathermolysis of heavy oil using a tri-metal supported zeolite catalyst

Yifeng Sun,[a] Shengke Li,*[a] Chuanmin Xiao,[b] Qicheng Liu,[b] Ding Wei[a] and Jiang Yang*[a]

A hierarchical zeolite-supported trimetallic catalyst (Mo/Co/Ni-ZSM-5) was synthesized *via* incipient wetness impregnation and evaluated for the hydrothermal upgrading of heavy oil. The catalytic system was designed to integrate acidic cracking functionality with metal-mediated hydrogenation under aquathermolysis conditions. Mono- and bimetallic counterparts were investigated for comparison. Among all tested catalysts, Mo/Co/Ni-ZSM-5 exhibited the highest hydrogenation activity and viscosity-reduction efficiency. Under optimized conditions (280 °C, 24 h, oil-to-water ratio of 7 : 3, and catalyst loading of 1.0 wt%), the heavy-oil viscosity decreased by 75.7%. Saturates, aromatics, resins, and asphaltenes (SARA) fractionation revealed an increase in saturates and aromatics and a reduction in resins and asphaltenes, accompanied by a significant reduction in sulfur and nitrogen contents. Spectroscopic analyses (FT-IR, ^{1}H-NMR, and GC-MS) demonstrated that catalytic upgrading proceeds *via* the fragmentation of condensed aromatic cores and deep hydrogenation. Crucially, the active hydrogen is supplied by a newly clarified dual-source pathway: tetralin acts as the primary donor, while high-temperature water serves as a synergistic hydrogen source *via* the catalytic water–gas shift reaction (WGSR). This combined active hydrogen supply ensures effective radical termination and prevents secondary condensation. Kinetic analysis indicated a low apparent activation energy of 16.87 kJ mol^{-1}, confirming the high catalytic efficiency of the trimetallic system. These results elucidate the synergistic roles of metal–acid bifunctionality, hierarchical porosity, and the complex catalytic function of water in heavy-oil aquathermolysis, providing practical guidance for the rational design of multifunctional catalysts.

Received 14th February 2026
Accepted 13th April 2026

DOI: 10.1039/d6ra01306f

rsc.li/rsc-advances

1. Introduction

Heavy oil resources represent more than 70% of the world's remaining petroleum reserves and are expected to play an increasingly important role in the global energy supply over the coming decades.[1,2] However, their exploitation and utilization are severely constrained by extremely high viscosity, which originates from the abundance of macromolecular components—particularly resins and asphaltenes—and the strong intermolecular interactions among these species, including hydrogen bonding and π–π stacking.[3,4] In addition, the high contents of heteroatoms such as sulfur and nitrogen further complicate upgrading processes and raise environmental concerns.[5–7]

Aquathermolysis, which utilizes high-temperature water or steam to promote *in situ* cracking and hydrogen transfer reactions, has emerged as a promising approach for heavy-oil upgrading. Nevertheless, non-catalytic aquathermolysis generally requires high temperatures and long reaction times and often suffers from limited viscosity reduction. The introduction of catalysts is therefore essential to lower activation barriers, enhance hydrogen transfer, and suppress secondary polymerization and coke formation.

ZSM-5 zeolite is widely employed in hydrocarbon conversion owing to its strong Brønsted acidity, shape selectivity, and hydrothermal stability. However, the intrinsic microporosity of conventional ZSM-5 severely restricts the diffusion of bulky heavy-oil molecules, leading to rapid deactivation and suboptimal performance. The development of hierarchical ZSM-5 with interconnected micro- and mesopores has proven effective in alleviating diffusion limitations and improving catalyst accessibility. Despite this structural advantage, purely acidic zeolites are insufficient to accomplish deep hydrogenation and heteroatom removal during heavy-oil upgrading.

To address these challenges, multifunctional catalysts integrating acidic and hydrogenation functionalities have been proposed.[8–10] Transition metals such as Mo, Co, and Ni are well-known for their hydrogenation, hydrodesulfurization, and hydronitrogenation activities. When combined with acidic zeolites, these metals can create synergistic bifunctional systems capable of saturating aromatic structures, cleaving heteroatom-containing bonds, and stabilizing cracked

[a]*College of Petrochemical Engineering, Liaoning Petrochemical University, Fushun 113001, China. E-mail: jyang98@126.com; Li_shengke@163.com; Tel: +86-24-56860789*

[b]*Institute of Exploration and Development, Liaohe Oilfield Company, Panjin 124010, China*

fragments.[11] Recent studies have shown that trimetallic systems outperform mono- or bimetallic catalysts by enhancing hydrogen utilization efficiency and suppressing coke formation under hydrothermal conditions.[12–14] Furthermore, nanoparticles generated from the *in situ* decomposition of water-soluble or oil-soluble metal precursors under hydrothermal conditions possess extremely high specific surface area and catalytic activity.[15]

In this work, a hierarchical ZSM-5-supported Mo/Co/Ni trimetallic catalyst was prepared *via* a simple impregnation–calcination route and systematically evaluated for heavy-oil aquathermolysis.[16,17] The catalyst structure and surface chemistry were characterized by XRD, BET, SEM, and XPS. Catalytic performance was assessed through viscosity measurements, SARA fractionation, elemental analysis, and kinetic modeling.[18] Moreover, the molecular-level evolution of heavy oil during upgrading was elucidated using FT-IR, ^{1}H NMR, and GC-MS. The study clarifies the structure–performance relationship of Mo/Co/Ni-ZSM-5 catalysts and provide mechanistic insight into their superior activity in hydrothermal heavy-oil upgrading.

2. Experimental section

2.1 Catalyst preparation and characterization

The typical preparation procedure is following: hierarchical ZSM-5 zeolite (Si/Al = 30–35, Nanjing Nengrui Technology Co., Ltd) was used as the support. Prior to impregnation, the zeolite was vacuum-dried at 120 °C for 6 h. Metal precursor solutions were prepared by dissolving ammonium heptamolybdate tetrahydrate, cobalt nitrate hexahydrate, and nickel nitrate hexahydrate (Aladdin Biochemical Technology Co., Ltd) in deionized water to achieve target metal loadings of 10 wt% Mo, 5 wt% Co, and 2 wt% Ni. The solution pH was adjusted to 4–5 using aqueous ammonia to prevent premature precipitation.[19]

The dried ZSM-5 support was added to the mixed precursor solution and stirred at room temperature for 2 h to ensure uniform impregnation. The resulting solid was filtered, washed with deionized water, and vacuum dried at 50 °C for 24 h. Calcination was performed in air at 550 °C for 4 h with a heating rate of 5 °C min^{-1}.[20] Mo/Co-ZSM-5 was prepared using the same procedure without the Ni precursor.

Catalysts were characterized by X-ray diffraction (XRD, D8 Advance, Bruker), N_2 adsorption–desorption (BET, ASAP 2020, Micromeritics), scanning electron microscopy (SEM, SU8010, Hitachi), and X-ray photoelectron spectroscopy (XPS, ESCALAB 250Xi, Thermo Fisher Scientific).

2.2 Heavy-oil characterization

Viscosity measurements were conducted using a rheometer equipped with a parallel-plate geometry at a fixed shear rate of 6 s^{-1}.[21] SARA fractionation was performed according to SY/T 5119-2008 to separate saturates, aromatics, resins, and asphaltenes.[22] Elemental analysis was used to determine C, H, N, and S contents, while oxygen was calculated by difference. The properties of the heavy oil before treatment are summarized in Table 1.

Table 1 Properties of the heavy oil

Property	Value
40 °C viscosity (mPa s)	100 237
Asphaltenes (wt%)	6.0
Saturates (wt%)	36.6
Aromatics (wt%)	21.6
Resins (wt%)	35.8
S (wt%)	0.581
N (wt%)	1.388
C (wt%)	86.578
H (wt%)	10.074
O (wt%)	1.379

The oil samples were characterized using the following techniques: Fourier transform infrared spectroscopy (FT-IR, FTIR-600 + 610, Agilent Technologies), proton nuclear magnetic resonance spectroscopy (^{1}H-NMR, AV 400, Bruker), and gas chromatography-mass spectrometry (GC-MS, 7890A, Agilent Technologies).

2.3 Catalytic aquathermolysis experiments

Catalytic aquathermolysis experiments were conducted in a high-pressure autoclave using 30 g of heavy oil from the Liaohe Oilfield. Deionized water was added at various oil-to-water ratios, and 1.0 mL of tetralin was used as a hydrogen-donor solvent.[23,24] The reactor was purged with nitrogen, pressurized to 3 MPa, and stirred at 500 rpm. Reactions were performed at temperatures ranging from 220 to 300 °C for different durations. After reaction, products were recovered for viscosity measurement and compositional analysis.

3. Results and discussion

3.1 Catalyst structure and surface properties

The prepared samples were shown in Fig. 1.

The SEM images in Fig. 2 show the morphology evolution of hierarchical ZSM-5 before and after metal–oxide loading. The untreated support mainly consists of quasi-spherical aggregates

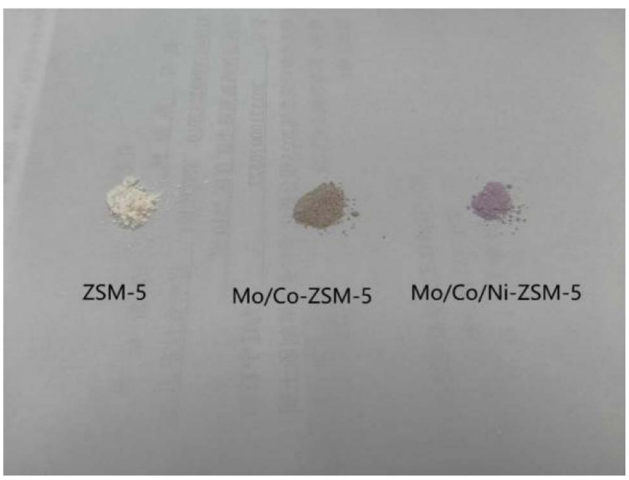

Fig. 1 ZSM-5, Mo/Co-ZSM-5 and Mo/Co/Ni-ZSM-5 samples.

(~5–80 μm) with rough edges and tightly packed microcrystals, and the alternating bright/dark regions suggest an internal meso-/macropore network that can facilitate precursor penetration (Fig. 2a and b). After co-impregnation and calcination at 550 °C, the overall particle shape is largely retained, but the surface becomes rougher with small granular protrusions, indicating deposition of the active phase near crystal boundaries; meanwhile, only slight pore narrowing is observed and no obvious melting or severe sintering appears (Fig. 2c). At higher magnification, bright nanoparticles are seen to be uniformly dispersed on the ZSM-5 surface, and the enhanced backscattered contrast from Ni/Co/Mo species supports that the oxides are anchored in a nanosized form, which is expected to improve thermal stability and sintering resistance (Fig. 2d).

Therefore, SEM images show that hierarchical ZSM-5 retains its aggregated morphology after metal loading, while nanosized metal oxide particles are uniformly dispersed on the zeolite surface.

BET results (Table 2) show how metal–oxide loading affects the pore structure of hierarchical ZSM-5. The parent ZSM-5 exhibits a high BET surface area of 441 $m^2\ g^{-1}$, a total pore volume of 0.31 $cm^3\ g^{-1}$, and an average pore size of 2.85 nm. After sequential impregnation and calcination with Mo/Co oxides, the surface area decreased to 357 $m^2\ g^{-1}$ and the pore volume to 0.25 $cm^3\ g^{-1}$, while the average pore size changed only slightly to 2.83 nm. With further introduction of Ni oxide, the surface area and pore volume decreased to 347 $m^2\ g^{-1}$ and 0.24 $cm^3\ g^{-1}$, respectively, and the average pore size remained nearly unchanged (2.81 nm).

Hence, BET analysis reveals a moderate decrease in surface area and pore volume after impregnation, indicating partial pore occupation without structural collapse.

Table 2 BET test data

Sample name	Specific surface area ($m^2\ g^{-1}$)	Pore volume ($cm^3\ g^{-1}$)	Aperture (nm)
ZSM-5	441.13	0.31	2.85
Mo/Co-ZSM-5	357.27	0.25	2.83
Mo/Co/Ni-ZSM-5	346.93	0.24	2.81

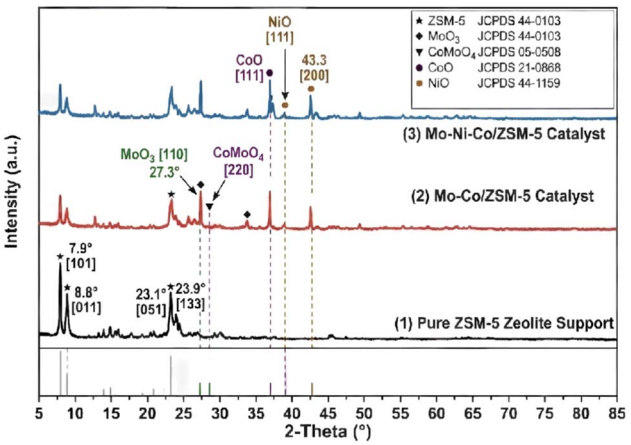

Fig. 3 XRD images of catalyst before and after loading (1) ZSM-5, (2) Mo/Co-ZSM-5, (3) Mo/Co/Ni-ZSM-5.

The XRD patterns (Fig. 3) show that the parent ZSM-5 (black curve) has typical diffraction peaks at $2\theta \approx 7.9°$, 8.9°, and 23.1°, and the sharp, intense reflections indicate a well-preserved zeolite framework with relatively high crystallinity. After

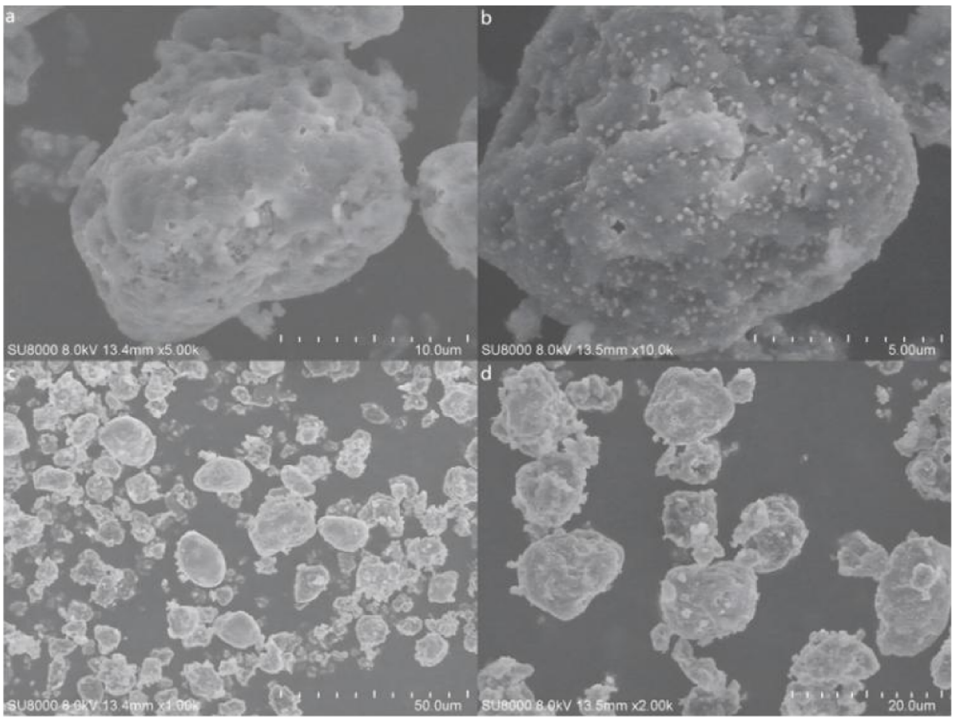

Fig. 2 SEM images of catalyst before and after loading (a and c: ZSM-5; b and d: Mo/Co/Ni-ZSM-5).

loading Mo and Co (red curve), the ZSM-5 characteristic peaks are still visible but with slight intensity changes, suggesting minor framework disturbance after impregnation/calcination. The retention of high crystallinity in the MFI framework post-modification aligns with recent findings by Schacht-Hernández *et al.* who demonstrated that hierarchical zeolites exhibit superior structural resilience against metal impregnation compared to their microporous counterparts. The slight attenuation in peak intensity observed here is consistent with the higher X-ray absorption coefficients of the heavy metal species relative to the aluminosilicate matrix, rather than a degradation of the zeolite lattice.[25] Meanwhile, new reflections appear at around $2\theta \approx 23°$, 33°, 37°, and 42°, which can be assigned to MoO_3 and CoO, and a peak near 27° is consistent with $CoMoO_4$, confirming the formation of oxide phases on the support. For Mo/Co/Ni-ZSM-5 (blue curve), additional peaks at about $2\theta \approx 37°$ and 43° match NiO, indicating that Ni is mainly present as an oxide, which may further tune the acidity and active-site distribution and benefit heavy-oil hydrothermal cracking.

Hence, XRD patterns confirm that the MFI framework of ZSM-5 is preserved, while reflections corresponding to MoO_3, CoO, $CoMoO_4$, and NiO are observed for the metal-loaded samples.

Finally, XPS was used to characterize the surface of catalyst as shown in Fig. 4. The XPS results indicate that Mo/Co/Ni-ZSM-5 contains abundant surface defects and mixed-valence metal species.[26,27] The O 1s spectrum (Fig. 4a) can be deconvoluted into lattice oxygen (O_L 530.9 eV), oxygen-vacancy-related oxygen (O_V 532.8 eV), and adsorbed oxygen/water (O_{abs} 533.4 eV). Compared with the parent ZSM-5, the higher O_V fraction suggests that metal loading and air calcination introduce more oxygen-vacancy defects, which may promote water activation under hydrothermal conditions; the strategic generation of oxygen vacancies (O_V 532.8 eV) is central to the mechanism of catalytic aquathermolysis. As elucidated in the 2024 study by Wang *et al.*,[28] surface oxygen vacancies on transition metal oxides act as Lewis acid sites that efficiently adsorb and dissociate water molecules, lowering the energy barrier for the generation of active hydrogen species and hydroxyl radicals. This correlates directly with the enhanced O_V fraction observed in our Mo/Co/Ni-ZSM-5 sample, suggesting that the catalyst is electronically primed to facilitate the water–gas shift reaction and hydrogen transfer pathways, which are essential for capping the radicals generated during heavy oil cracking.[29] The presence of O_{abs} also implies enhanced surface hydrophilicity, benefiting mass transfer at the oil–water interface. In the Mo 3d region (Fig. 4b), peaks at 232.9 eV (Mo^{6+}) and 231.5 eV (Mo^{5+}) with an area ratio of 1.6 : 1 confirm the coexistence of a Mo^{6+}/Mo^{5+} redox pair, likely related to electron transfer and/or partial oxygen deficiency and favorable for hydrogen-transfer processes. The Co 2p spectrum (Fig. 4c) shows Co^{3+} (780.99 eV) and Co^{2+} (783.14 eV) with clear satellite features, which is consistent with a defect-rich Co_3O_4-like phase. The Ni signal is relatively weak due to its low content; however, the Ni 2p region (Fig. 4d) still shows peaks at 855.9 and 873.1 eV with a shake-up satellite, indicating that Ni mainly exists as Ni^{2+}.[30,31]

Hence, XPS analysis demonstrates the coexistence of mixed-valence Mo and Co species and abundant surface oxygen vacancies, which are conducive to water activation and hydrogen transfer under hydrothermal conditions.

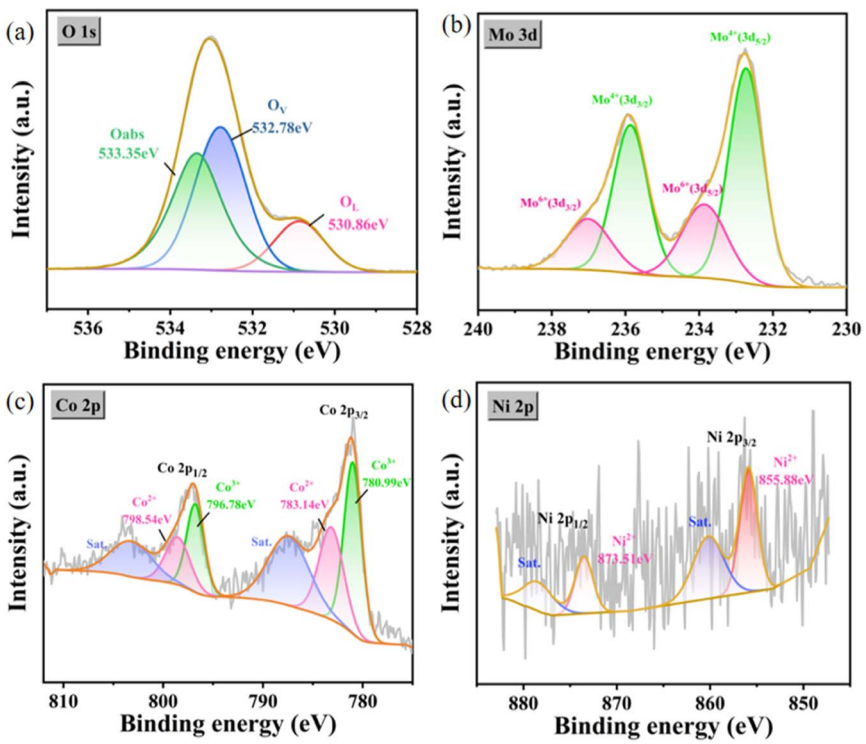

Fig. 4 XPS plots of Mo/Co/Ni-ZSM-5 catalysts.(a) O 1s, (b) Mo 3d, (c) Co 2p, and (d) Ni 2p regions.

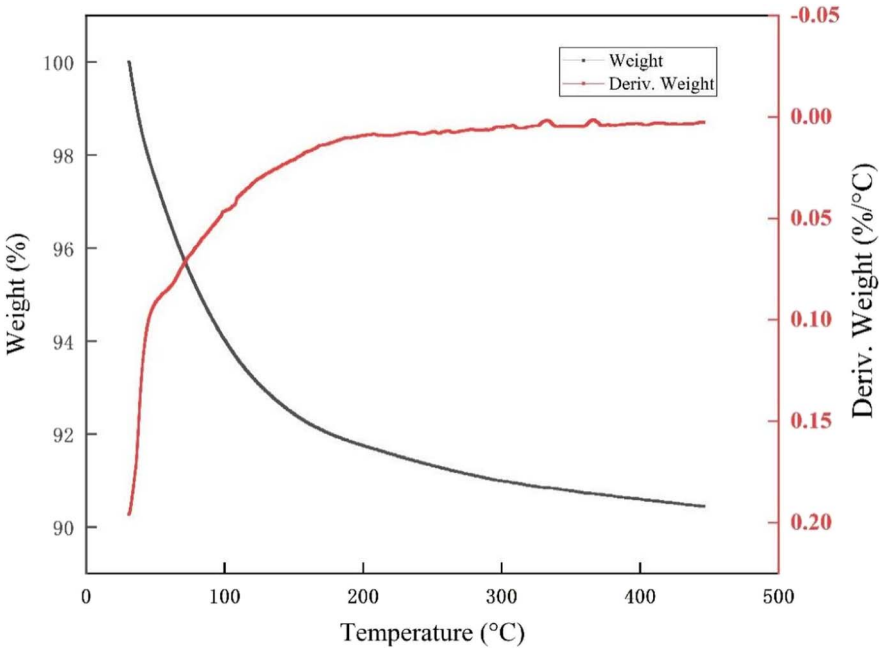

Fig. 5 Thermogravimetric curve of Mo/Co/Ni-ZSM-5 catalyst.

Thermogravimetric analysis (TGA) reveals that the trimetallic supported ZSM-5 catalyst exhibits a total weight loss of approximately 9 wt% from 30 °C to 450 °C, with the primary mass loss occurring between 30 °C and 250 °C. Specifically, the initial weight loss of 4 wt% from 30 °C to 120 °C is mainly attributed to the desorption of physically adsorbed and weakly coordinated water. The subsequent 2 wt% loss in the range of 120–250 °C corresponds to the removal of coordinated water from the metal precursors and the condensation–dehydration of surface hydroxyl groups. The 3 wt% loss observed between 250 °C and 400 °C is likely due to the deep dehydroxylation of the ZSM-5 framework and the complete thermal decomposition of residual organic ligands. Above 400 °C, the TGA curve plateaus, indicating excellent structural and thermal stability of the catalyst up to 450 °C (Fig. 5).

3.2 Catalytic performance and reaction optimization

To accurately evaluate the intrinsic contribution of the designed catalysts, non-catalytic control experiments were conducted under identical optimized conditions (280 °C, 24 h, oil-to-water ratio of 7 : 3). As presented in Table 3, the raw heavy oil exhibited an initial viscosity of 100 237 mPa s. In the pure aquathermolysis system (heavy oil + deionized water) without any catalyst or hydrogen donor, the viscosity was reduced to 75 963 mPa s, corresponding to a viscosity reduction rate of 24.2%.

When 1 mL of tetralin was introduced into the non-catalytic system as a hydrogen donor, the viscosity was further reduced to 68 479 mPa s. Although the addition of tetralin slightly improved the removal of heteroatoms and marginally reduced the asphaltene content to 5.9 wt%, the H/C atomic ratio plateaued at 1.390, nearly identical to the water-only system. These results demonstrate that while the hydrogen donor can partially stabilize thermal radicals to prevent condensation, its hydrogen-donating efficiency and the subsequent deep hydrogenation of heavy fractions are severely restricted in the absence of a catalyst. Consequently, a baseline viscosity reduction of ~31% is established for the non-catalytic thermal and hydrogen-donor effects, underscoring the necessity of introducing the Mo/Co/Ni-ZSM-5 catalyst to achieve deep upgrading.

As shown in Table 4 under oil-to-water ratio of 7 : 3, and 1.0 mL of tetralin as a hydrogen-donor solvent, compared with bare ZSM-5, Mo/Co-ZSM-5 exhibits markedly enhanced viscosity reduction due to improved hydrogenation activity. The trimetallic Mo/Co/Ni-ZSM-5 catalyst delivers the best

Table 3 The effect of adding hydrogen donors on viscosity reduction of heavy oil

Reactant	Viscosity (40 °C, mPa s)	Viscosity reduction (%)	Asphaltenes (wt%)	Saturates (wt%)	Aromatics (wt%)	Resins (wt%)	S (wt%)	N (wt%)	C (wt%)	H (wt%)	H/C
Heavy oil	100 237	—	6.0	36.6	21.6	35.8	0.58	1.39	86.58	10.07	1.386
Heavy oil + deionized water	75 963	24.2	5.9	36.8	21.8	35.5	0.55	1.32	86.61	10.09	1.388
Heavy oil + deionized water + tetralin	68 479	31.7	5.9	37.0	21.7	35.4	0.53	1.31	86.65	10.11	1.390

Table 4 Effects of different catalysts at 280 °C for 24 h

Catalyst types	Viscosity (40 °C, mPa s)	Viscosity reduction (%)	Asphaltenes (wt%)	Saturates (wt%)	Aromatics (wt%)	Resins (wt%)	S (wt%)	N (wt%)	C (wt%)	H (wt%)	H/C
ZSM-5	64 701	35.5	5.9	36.9	22.0	35.2	0.54	1.30	86.74	10.11	1.389
Mo/Co-ZSM-5	30 564	69.5	5.1	38.9	22.8	33.2	0.36	0.98	87.33	10.33	1.409
Mo/Co/Ni-ZSM-5	24 320	75.7	4.8	39.1	23.6	32.5	0.35	0.95	87.51	10.39	1.415

performance, achieving a viscosity reduction of 75.7% at 280 °C for 24 h with a catalyst loading of 1.0 wt%. In contrast to the non-catalytic system, the introduction of the Mo/Co/Ni-ZSM-5 catalyst led to a noticeable conversion of heavy fractions. Specifically, the asphaltene and resin contents decreased to 4.8 wt% and 32.5 wt%, respectively, accompanied by an increase in saturates to 39.1 wt%. Concurrently, the H/C atomic ratio significantly improved to 1.415. These substantial compositional shifts, coupled with the sharp decline in sulfur and nitrogen contents, clearly demonstrate that the tri-metallic catalyst not only efficiently cleaves the heteroatom-containing weak bonds but also strongly promotes the deep hydrogenation and fragmentation of the macromolecular frameworks of asphaltenes and resins.

Optimization studies in Table 5 indicate that while the absolute viscosity reduction continues to increase at higher reaction severities, severe diminishing returns are observed beyond certain thresholds. From a techno-economic perspective, the 'optimum' condition is determined by balancing catalytic efficiency against energy consumption and equipment throughput. For instance, increasing the water–oil ratio from 7 : 3 to 5 : 5 only yields a marginal 4.4% additional viscosity reduction (from 75.7% to 80.1%), but requires heating a substantially larger volume of water, which possesses a high specific heat capacity and latent heat, thereby drastically increasing energy costs. Similarly, increasing the temperature to 300 °C or doubling the reaction time to 48 h only provides negligible improvements while requiring more demanding reactor pressure ratings and halving the operational throughput. Therefore, comprehensive consideration of both performance and economic feasibility establishes 280 °C, 24 h, and an oil-to-water ratio of 7 : 3 as the practical optimal conditions for this catalytic system. The significant reduction in viscosity, coupled with the transition from heavy fractions to light fractions (saturates and aromatics), acts as a direct and robust indicator of the macroscopic upgrading and lightening of the heavy oil.

These results suggest that ZSM-5 with only acidic sites provides a certain cracking ability, while introducing Mo/Co significantly improves hydrogenation activity. The ternary catalyst delivered the best performance due to the synergy between the metal–acid bifunctional sites and the hierarchical pore channels. With this catalyst, aqueous phase and hydrogen-donor, viscosity reduction and heteroatom removal can be achieved without a large increase in energy input.

3.3 Aquathermolysis degradation of heavy oil

The quantitative separation of the four SARA fractions (saturates, aromatics, resins, and asphaltenes) for both the raw and

Table 5 Effects of various reaction parameters on the viscosity reduction of heavy oil

Reaction parameter	Value	Viscosity (40 °C, mPa s)	Viscosity reduction (%)
Catalyst dosage, wt%	0 (no catalyst)	75 963	24.2
	0.1	50 752	49.4
	0.5	31 247	68.8
	1.0	24 320	75.7
	2.0	21 175	78.9
Reaction temperature, °C	220	33 902	66.2
	240	29 132	70.9
	260	26 071	73.9
	280	24 320	75.7
	300	23 684	76.4
Reaction time, h	6	41 481	58.6
	12	35 739	64.4
	18	29 475	70.7
	24	24 320	75.7
	48	22 500	77.5
Water/oil ratio	9 : 1	50 394	49.5
	8 : 2	32 368	66.3
	7 : 3	24 320	75.7
	6 : 4	21 009	79.0
	5 : 5	19 947	80.1

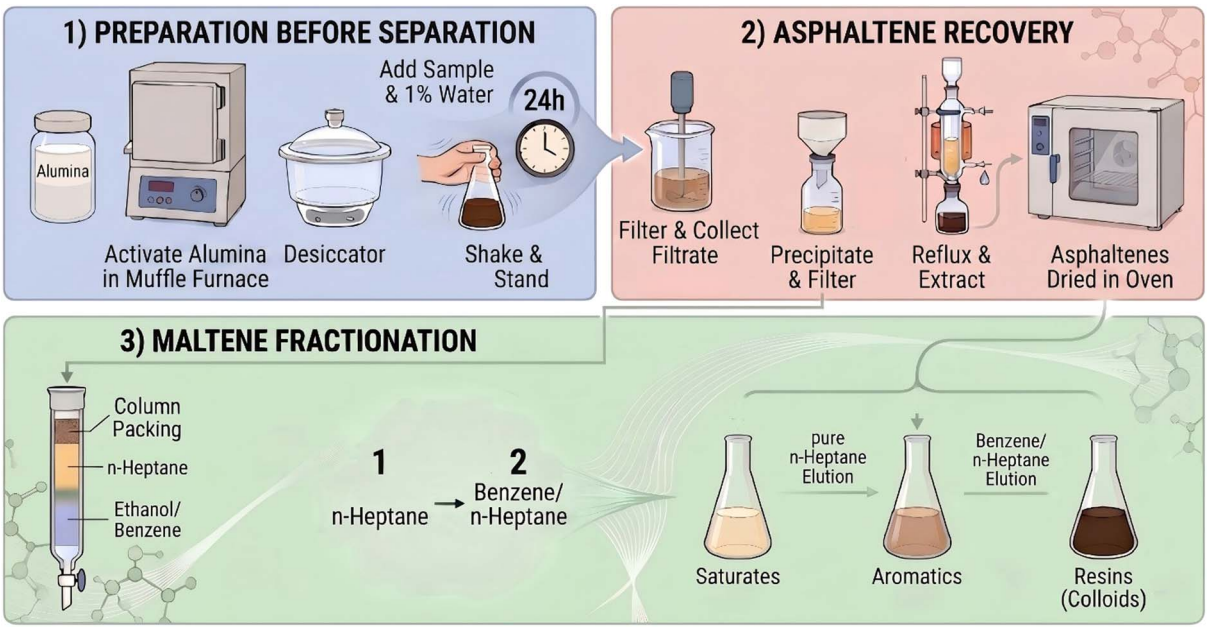

Fig. 6 Four-component separation process diagram.

upgraded heavy oil was conducted strictly following the standard method: NB/SH/T 0509-2010. First, an excess amount of *n*-heptane was added to the oil sample to completely precipitate the asphaltenes (defined as C_7-asphaltenes). The precipitated C_7-asphaltenes were then filtered, washed, and subsequently purified *via* Soxhlet extraction using toluene. After the extraction, the solvent was removed from the initial *n*-heptane filtrate to obtain the deasphalted maltenes. The maltenes were then loaded onto a glass chromatographic column packed with neutral alumina and silica gel. The column was sequentially eluted using solvents with increasing polarity: *n*-hexane was used to elute the saturates; toluene was used to elute the aromatics; and finally, a mixture of toluene and absolute ethanol was used to elute the resins. The respective eluents were collected, the solvents were evaporated, and each fraction was accurately weighed to calculate its mass percentage. The specific process is shown in Fig. 6, and the actual diagram is shown in Fig. 7.

Fig. 7 The four fractions separated by column chromatography elution (the image displays SARA fractions as solutions in their respective extraction/elution solvents prior to rotary evaporation and drying) (from left to right: asphaltene, saturated, aromatic, and resins).

FT-IR spectrum was used to analysis of crude oil before and after the reaction. The FT-IR spectra suggest clear structural changes in the oil after catalytic upgrading (Fig. 8). Strong CH_3 and CH_2 stretching bands in the 2800–3000 cm^{-1} region were observed for the oil before reaction, indicating a high content of long-chain alkanes. After reaction, the overall intensity in this region slightly decreased and the CH_3 contribution became relatively more pronounced, implying that long-chain alkanes were decomposed into shorter and more branched hydrocarbons in the presence of Mo/Co/Ni-ZSM-5 as a catalyst. This spectral evolution is the same as the findings of Wang *et al.* (2024)[28] in the aquathermolysis of extra-heavy oil, where a similar attenuation of methylene ($-CH_2-$) vibration bands was quantitatively linked to the catalytic rupture of long alkyl side chains attached to asphaltene cores. The preferential preservation and relative intensity increase of methyl ($-CH_3$) signals further corroborate the mechanism of β-scission catalyzed by the strong Brønsted acid sites of the hierarchical ZSM-5. This mechanism converts waxy, long-chain paraffins into lighter, branched isomers, which is a primary driver for the significant reduction in the pour point and viscosity of the upgraded crude.[32] The C=C band around 1600–1700 cm^{-1} became slightly stronger in the product oil, suggesting that acidic sites promoted partial dehydrogenation of alkanes to form olefinic/aromatic structures. Consistently, the bands at 1450 and 1375 cm^{-1} (CH_2 bending and CH_3 symmetric bending) showed a more evident CH_3 signal and a relatively weaker CH_2 signal, further supporting chain scission and oil lightening. In

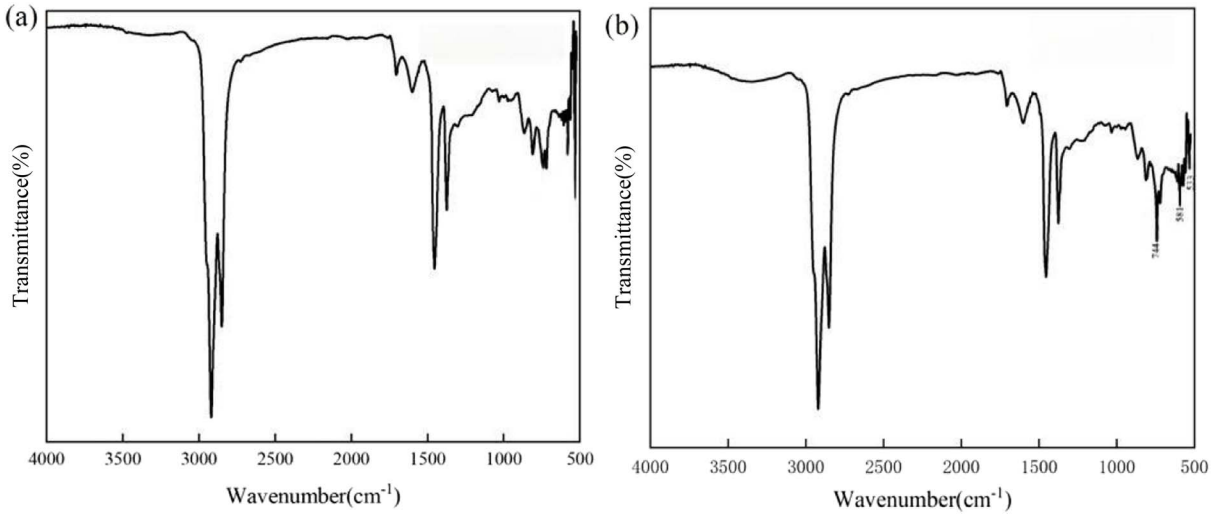

Fig. 8 (a) FT-IR image of heavy oil; (b) FT-IR image of oil after Mo/Co/Ni-ZSM-5 catalytic reaction.

contrast, the 1000–1300 cm^{-1} region changed little, indicating that the products remained mainly hydrocarbons without obvious formation of new oxygen-containing functionalities. In the low-wavenumber region, the bands at 744, 581, and 533 cm^{-1} increased to different extents, with more noticeable enhancement at 744 and 581 cm^{-1}, which is consistent with increased aromatic-ring-related vibrations and suggests dehydrogenation cyclization/aromatization reactions. The relatively small change at 533 cm^{-1} implies that the formed aromatics were mainly mono- or bicyclic species, while the formation of polycyclic aromatics and coke was suppressed. Overall, the catalyst promotes cracking, dehydrogenation, and aromatization of heavy fractions, leading to a lighter and more aromatic product oil.[33,34]

Therefore, FT-IR analysis indicates the cracking of long alkyl chains and the formation of shorter, more branched hydrocarbons, while excessive polyaromatic condensation is suppressed.

^{1}H-NMR spectrum was also used to compare structure of asphaltenes in oil before and after the reaction. The ^{1}H NMR spectra provide information on the hydrogen environments in the molecules, and the assignments were made by combining chemical shifts, splitting features, and integrated peak areas.[35] In particular, the protons on alkyl chains and aromatic rings show distinct chemical-shift ranges, which allows them to be differentiated and quantified. Based on the structural parameters proposed by Brown and Ladner, including aromaticity (f_A) and the aromatic condensation index (H_{Au}/C_A), these parameters were calculated using eqn (1) and (2), together with the corresponding chemical-shift regions. In addition, following the classification approach reported in the literature for aromatic condensed structures, the protons detected in the asphaltene fraction were grouped according to their spatial positions and chemical environments and were denoted as H_A, H_α, H_β, and H_γ (Fig. 9 and Table 6).[36]

$$f_A = \frac{C_T/H_T - (H_\alpha + H_\beta + H_\gamma)/2H_T}{C_T/H_T} \quad (1)$$

$$H_{Au}/C_A = \frac{H_A/H_T + H_\alpha/2H_T}{C_T/H_T - (H_\alpha + H_\beta + H_\gamma)/2H_T} \quad (2)$$

In the eqn (2): C_T—the total number of carbon moles (mol); H_T—the total number of hydrogen moles (mol).

Given the intricate composition of heavy oil, relying on single-method analysis often falls short in capturing the full structural evolution during upgrading.[37] Here, ^{1}H-NMR characterization reveals that hydrothermal cracking triggers a fundamental restructuring of the asphaltene fraction. In Fig. 10, Tables 7 and 8, while the virgin asphaltenes exhibited a typical aromatic-rich core ($H_\alpha \sim 18.5\%$) with moderate alkyl

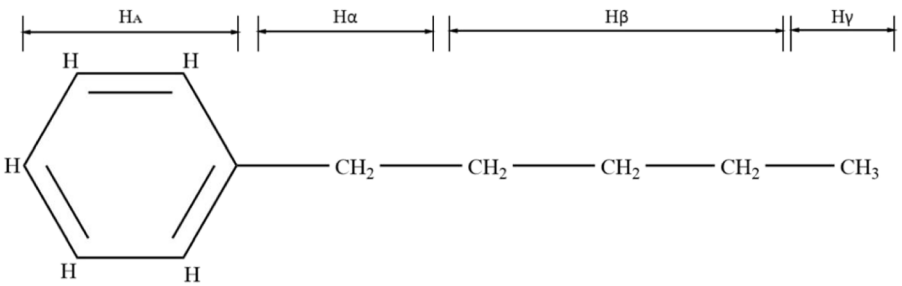

Fig. 9 Schematic diagram of the assignment of hydrogen NMR spectrum of heavy oil.

Table 6 Chemical shifts of different types of H in ^{1}H-NMR

Parameter	Different types of H	Chemical shift (ppm)
H_A	H directly bonded to aromatic carbon	6.0–9.0
H_α	H attached to the α carbon of the aromatic ring	2.0–4.0
H_β	H on CH_2 at the β position and outside the β position of the aromatic ring, and H on CH	1.0–2.0
H_γ	H on CH_3 outside the γ position of the aromatic ring	0.5–1.0

substitution, the introduction of the Co/Ni-ZSM-5 catalyst drastically shifted this distribution. We observed a collapse in aromatic protons (H_A) to 5.90% alongside a surge in methylene protons (H_β) to 76.64%, marking a clear transition from polycyclic aromatic networks to saturated, aliphatic-dominant structures. The drastic reduction in aromaticity (f_A) from 0.557 to 0.198 is a standout result that exceeds typical thermal cracking baselines. Recent ^{1}H-NMR studies by Krivdin (2024)[38] on asphaltene subfractions emphasize that such a collapse in f_A is only achievable through deep catalytic hydrogenation, where the metal functionality (Mo/Co/Ni) actively saturates the peripheral aromatic rings, rendering them susceptible to subsequent ring-opening by the zeolite's acid sites. This synergistic "saturate-then-crack" pathway effectively converts the refractory aromatic core into hydrogen-rich alkyl fragments, significantly increasing the H/C ratio of the final product.[39,40] This 64% drop in aromaticity (f_A), coupled with an increased H/C ratio, confirms that the process goes beyond simple cracking; it involves deep hydrogenation and ring opening where aromatic cores are effectively converted into long-chain alkanes. Crucially, the rise in the aromatic condensation index (H_{Au}/C_A) further elucidates a "fragmentation" of the aromatic cores, indicating a shift from large condensed clusters to smaller mono- or di-cyclic units. This transformation is driven by the synergistic architecture of the Mo/Co/Ni-ZSM-5 catalyst, where metal species facilitate C–C and C–S bond scission while the zeolite acid sites promote the skeletal rearrangement and dearomatization necessary for substantial viscosity reduction.

Therefore, ^{1}H NMR analysis of asphaltenes reveals a dramatic decrease in aromatic proton content and aromaticity (f_A), accompanied by an increase in aliphatic hydrogen, indicating deep hydrogenation and fragmentation of condensed aromatic cores.

Finally, GC-MS was used to determine saturated fractions before and after reaction. The chromatogram of the initial heavy oil (Fig. 11a) is characterized by a broad, continuous envelope of dense peaks spanning 5–35 min, signaling the dominance of high-molecular-weight linear and cycloalkanes. In stark contrast, catalytic upgrading over Mo/Co/Ni-ZSM-5 (Fig. 11b) triggers a fundamental shift in this distribution: the heavy "tail" (20–35 min) recedes significantly, giving way to a surge in signal intensity at the lighter end (5–12 min). Quantitative analysis of this shift reveals a marked increase in the concentration of *n*-C_{10} to *n*-C_{20} alkanes. This distribution profile is highly concordant with recent GC-MS data from catalytic aquathermolysis studies by Maity *et al.* (2025),[41] where the interaction of superheated steam with transition metal catalysts was shown to selectively cleave the C_α–C_β bonds in alkyl–aromatic structures. Crucially, the enhanced yield of light saturates serves as direct evidence that the Mo/Co/Ni-ZSM-5 catalyst not only cracks heavy molecules but also effectively utilizes *in situ* generated hydrogen to terminate the resulting alkyl radicals. This radical termination step is vital, as noted by Kholmurodov *et al.* (2025),[42] for suppressing the retro-polymerization of cracked fragments into coke. This overall migration toward shorter retention times provides direct evidence of long-chain scission. Moreover, the evolution of fine, dispersed peak clusters in the 8–12 min region underscores a synergy between ZSM-5-mediated cracking and isomerization—where the cleavage of C–C bonds in heavy *n*-alkanes is coupled with the formation of iso-alkanes and naphthenes, effectively converting heavy macromolecules into high-value, light hydrocarbons.[43]

Hence, GC-MS results further confirm a shift in the saturated fraction toward lighter *n*-alkanes (C_{10}–C_{20}), demonstrating effective chain scission and radical stabilization.

3.4 Kinetic analysis

To quantitatively evaluate the catalytic efficiency of the Mo/Co/Ni-ZSM-5 system, a lumped kinetic model was applied to the hydrothermal cracking process. Assuming the viscosity reduction follows a pseudo-first-order reaction mechanism, the reaction rate constant (k) can be expressed as:

$$\ln\left(\frac{\mu_0 - \mu_{\lim}}{\mu_t - \mu_{\lim}}\right) = k \times t \tag{3}$$

where μ_0, μ_t and $\mu_{\lim}$ represent the initial viscosity, the viscosity at reaction time t, and the limiting viscosity (viscosity of light oil limit), respectively. Based on the experimental data at different temperatures (Table 5), the apparent activation energy (E_a) was calculated using the Arrhenius equation:

$$\ln k = \ln A - \frac{E_a}{RT} \tag{4}$$

Fig. 12 presents the Arrhenius plot of $\ln k$ *versus* $1000/T$. The plot exhibits an excellent linear relationship with a determination coefficient R^2 of 0.97, confirming that the viscosity reduction follows pseudo-first-order kinetics. The Arrhenius plot yields an apparent activation energy E_a of 16.87 kJ mol^{-1}, substantially lower than that of non-catalytic aquathermolysis (often > 50 kJ mol^{-1}), highlighting the efficiency of the Mo/Co/Ni-ZSM-5 catalyst in lowering energy barriers for heavy-oil upgrading, and effectively facilitates the cleavage of C–S and C–C bonds at relatively mild temperatures (280 °C). The

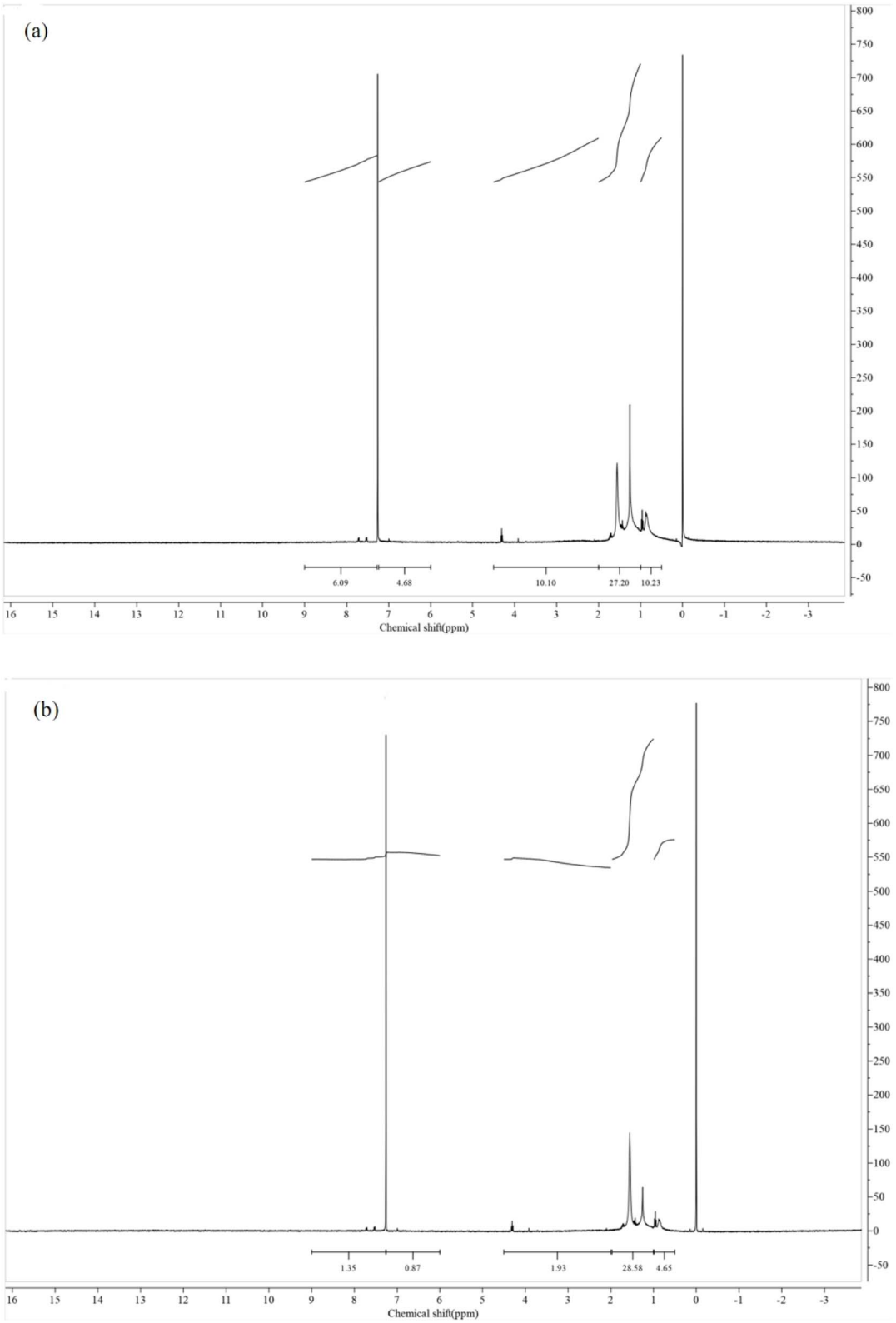

Fig. 10 (a) ^{1}H-NMR spectrum of asphaltenes from heavy oil; (b) ^{1}H-NMR spectrum of asphaltenes from oil after the Mo/Co/Ni-ZSM-5 catalytic reaction.

relatively low E_a value suggests that the catalytic reaction is highly efficient, possibly approaching the diffusion-limited regime where mass transfer becomes significant. Consequently, the Mo/Co/Ni-ZSM-5 system accelerates the conversion of macromolecular asphaltenes into lighter fractions, leading to the substantial viscosity reduction observed.

Table 7 The percentage of integral area of different types of hydrogen in the asphaltenes of heavy oil after the catalytic reaction of Mo/Co/Ni-ZSM-5

Sample	H_A	H_α	H_β	H_γ
Heavy oil asphaltene	18.47	17.33	46.65	17.55
Asphaltene after Mo/Co/Ni-ZSM-5 catalytic reaction	5.90	5.13	76.64	12.34

Table 8 C_T/H_T, f_A, and H_{Au}/C_A of asphaltenes in heavy oil after catalytic reaction with Mo/Co/Ni-ZSM-5

Sample	C_T/H_T	f_A	H_{Au}/C_A
Heavy oil asphaltene	0.921	0.557	0.695
Asphaltene after Mo/Co/Ni-ZSM-5 catalytic reaction	0.586	0.198	0.730

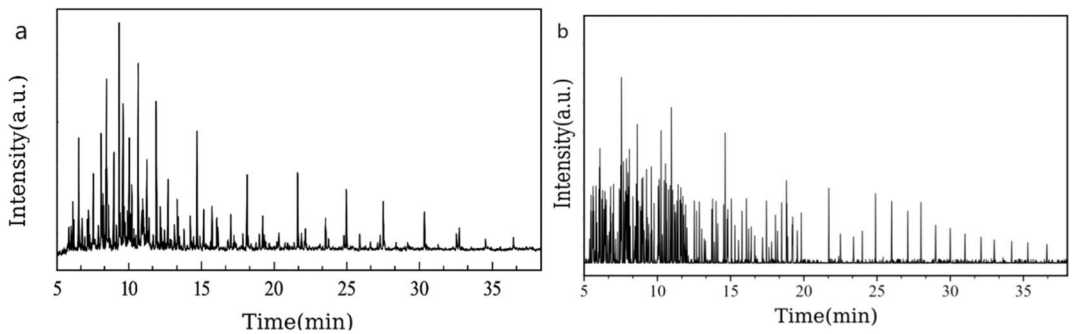

Fig. 11 (a) GC-MS diagram of saturated fractions in heavy oil; (b) GC-MS diagram of saturated fractions in oil after Mo/Co/Ni-ZSM-5 catalytic reaction.

3.5 Reaction mechanism

Based on the catalytic performance and spectroscopic characterization results discussed above, a tentative mechanism for the aquathermolysis of heavy oil over the hierarchical Mo/Co/Ni-ZSM-5 catalyst is proposed, as illustrated in Fig. 13. The upgrading process involves a synergistic interplay between the hierarchical porosity, Brønsted acidity, and metal-mediated hydrogenation functionalities.

The most critical aspect of this mechanism is the synergy between cracking and hydrogenation. The thermal and catalytic

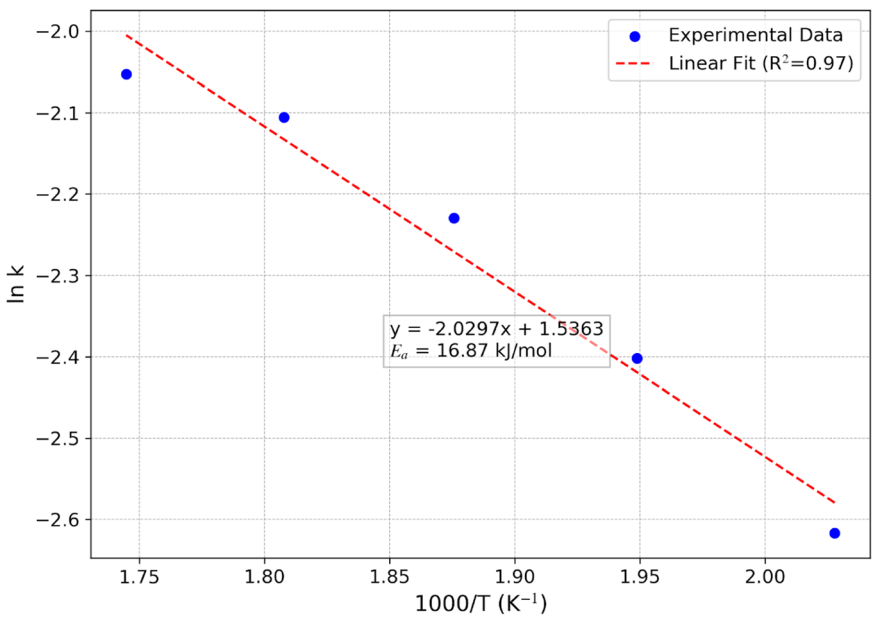

Fig. 12 Arrhenius plot of ln k *versus* 1000/T for the viscosity reduction of heavy oil over the Mo/Co/Ni-ZSM-5 catalyst (R^2 = 0.97).

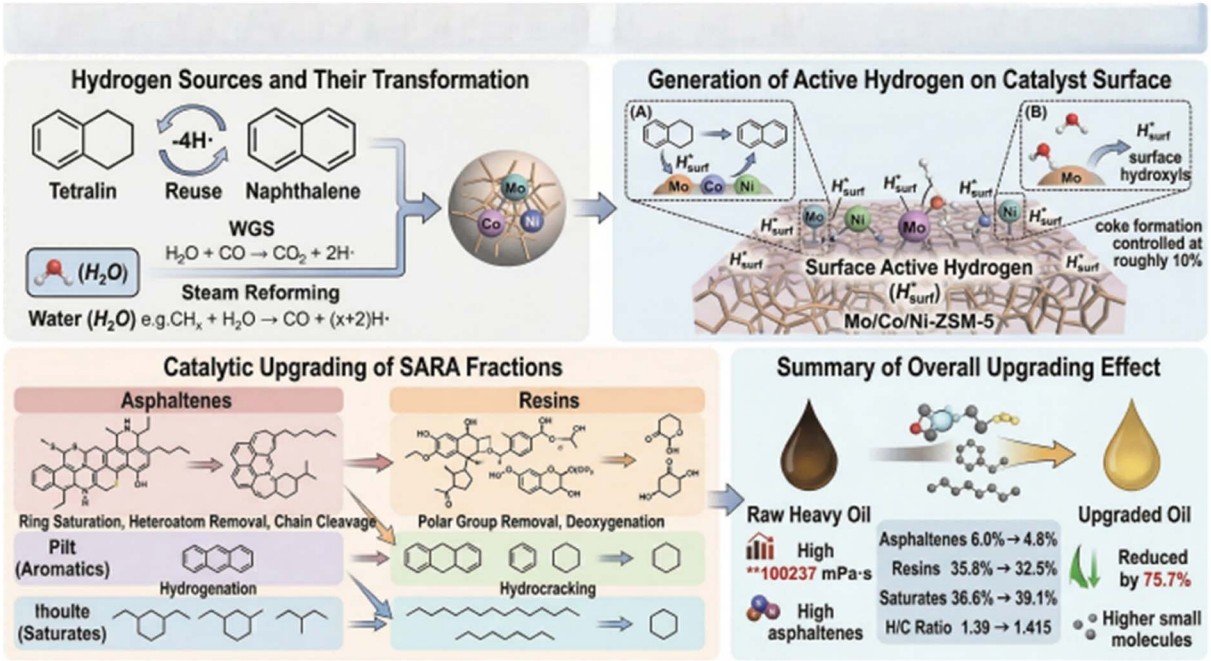

Fig. 13 Mechanism of Mo/Co/Ni-ZSM-5 catalyst.

cracking of heavy molecules generates free radicals. In the absence of sufficient hydrogen, these radicals would rapidly recombine to form larger coke precursors. However, in the Mo/Co/Ni-ZSM-5 system, the metal sites ensure a steady supply of active hydrogen to immediately cap and stabilize these free radicals. This "cracking-hydrogenation" balance effectively converts the heavy asphaltene/resin fractions into lighter saturates and aromatics.

The multifaceted role of water in the catalytic system. It is essential to clarify the specific roles of water in this aquathermolysis system at 280 °C. Thermodynamically, the direct thermal splitting of water into molecular hydrogen is impossible at this temperature. Consequently, the added tetralin serves as the primary and dominant hydrogen donor. The most universally accepted role of high-temperature steam in this process is hydrolysis. Water actively participates in the hydrolytic cleavage of weak heteroatomic bridges connecting the polycyclic aromatic sheets in heavy oil, directly contributing to viscosity reduction. Furthermore, in the presence of the multimetallic Mo/Co/Ni-ZSM-5 catalyst, water is proposed to act as an indirect synergistic hydrogen source *via* the catalytic water–gas shift reaction (WGSR). According to classical aquathermolysis mechanisms, the initial cleavage of heteroatom-containing macromolecules generates light fragments and carbon monoxide. The metallic active sites highly promote the reaction between this CO and water. Through this pathway, water indirectly provides active hydrogen to stabilize cracked radicals and promote further hydrodesulfurization. While the significant upgrading performance supports this synergistic WGSR mechanism, definitively quantifying the proportion of hydrogen donated by water requires isotopic labeling tracers. Future mechanistic investigations employing D_2O are planned to strictly track the direct incorporation of water-derived hydrogen into the hydrocarbon matrix.

4. Conclusions

A hierarchical Mo/Co/Ni-ZSM-5 catalyst was successfully developed for the efficient aquathermolysis of heavy oil. Under optimized mild conditions (280 °C, 24 h), the catalytic system demonstrated exceptional performance, achieving a significant viscosity reduction of 75.7%. Comprehensive characterizations (FT-IR, ^{1}H-NMR, GC-MS) and SARA fractionation confirmed that the catalyst effectively promotes the conversion of heavy asphaltene and resin fractions into lighter hydrocarbons. Mechanistically, the trimetallic system exhibits strong metal–acid synergy that drives a newly clarified dual-hydrogen-source upgrading pathway. While tetralin acts as the primary hydrogen donor, high-temperature water serves as a synergistic hydrogen source *via* the catalytic water–gas shift reaction (WGSR). This combined active hydrogen supply rapidly stabilizes cracked radicals, enabling deep hydrogenation and aromatic core fragmentation while effectively suppressing secondary condensation into coke. Furthermore, kinetic analyses demonstrated that the catalyst significantly lowers the activation energy of the viscosity reduction process. Ultimately, this study provides profound mechanistic insights—particularly clarifying the complex catalytic role of water—and offers practical guidance for the design of multifunctional catalysts for *in situ* and *ex situ* heavy oil upgrading.

Conflicts of interest

The authors declare no competing financial interest.

Data availability

All data generated or analyzed during this study are included in this published article.

Acknowledgements

This work was supported by the Liaoning Revitalization Talents Program (project no. XLYC1902053), the Science and Technology Research Project of Liaoning Provincial Department of Education (no. JYTMS20231440), and the National Science and Technology Major Project for New Oil and Gas Exploration and Development (no. 2025ZD1407602).

References

1 A. R. H. Goodwin, The Future of Oil and Gas Fossil Fuels, in *Future Energy: Improved, Sustainable and Clean Options for Our Planet*, ed. T. M. Letcher, Elsevier, Amsterdam, 2008, pp. 3–24.

2 Z. Liu, H. Wang, G. Blackbourn, F. Ma, Z. He, Z. Wen and Z. Wu, Heavy Oils and Oil Sands: Global Distribution and Resource Assessment, *Acta Geol. Sin. (Engl. Ed.)*, 2019, **93**, 199–212.

3 M. A. Hanfi, O. S. Alade, A. Tanimu, M. Mahmoud and S. A. Alarifi, Catalytic and Noncatalytic in Situ Hydrogen Production from Heavy Oil: A Review of Experimental Studies, *ACS Omega*, 2024, **9**(51), 50118–50133.

4 R. Marquez, C. Ovalles, F. Lopez-Linares, W. Wang, P. Robinson and M. A. Reynolds, Perspective from the ACS Energy & Fuels Industry Committee toward the Transition to Sustainable Energy Sources, *Energy Fuels*, 2025, **39**(3), 1451–1459.

5 E. A. Taborda, I. Moncayo-Riascos, M. Riazi, C. A. Franco and F. B. Cortés, Elucidating the Nanoparticle–Asphaltene–Resin Interactions and Their Effect on Heavy Crude Oil Viscosity Changes, *Energy Fuels*, 2025, **39**(1), 247–259.

6 Q. H. Zhao, J. X. Wu, T. H. Zhou, S. Q. Zhao and Q. Shi, Impact of molecular composition on viscosity of heavy oil: Machine learning based on semi-quantitative analysis, *Fuel*, 2024, **368**, 131616.

7 L. Prada, J. Botett, M. D. Contreras-Mateus, A. Hethnawi, S. S. Baakeem and N. N. Nassar, Nanoparticles Technology for Improving Steam-Assisted Gravity Drainage Process Performance: A Review, *Ind. Eng. Chem. Res.*, 2024, **63**(30), 13047–13077.

8 L. Wei, H. Wang, Q. Dong, Y. Li and H. Xiang, A Review on the Research Progress of Zeolite Catalysts for Heavy Oil Cracking, *Catalysts*, 2025, **15**(4), 401.

9 P. Wang, J. Wang, X. Shu, M. Bian, X. Xiao, X. Fan, L. Kong, Z. Xie and Z. Zhao, Rapid Synthesis of Self-Pillared ZSM-5 Zeolite Nanosheets with Enhanced Catalytic Performance in n-Octane Cracking, *Ind. Eng. Chem. Res.*, 2024, **63**(44), 18773–18782.

10 E. N. Al-Shafei, Z. Qureshi, M. Z. Albahar, A. Alasseel, S. Asaoka and A. Aitani, Hierarchical ZSM-5@SiO_2 Catalysts: A Novel Approach to Optimizing Olefin Yield from Heavy Atmospheric Gas Oil, *J. Phys. Chem. C*, 2024, **128**(25), 10440–10449.

11 F. Aliev, Y. Abdelsalam, S. Lapuk, M. A. Khelkhal, M. Suwaid and A. Vakhin, Efficient Heavy Oil Upgrading with Water-Soluble Nickel and Copper Acetate Catalysts, *Ind. Eng. Chem. Res.*, 2024, **63**(15), 6546–6561.

12 K. K. Urazov, N. N. Sviridenko, E. N. Kolobova and M. V. Grabchenko, Nickel-Cobalt Sulfide Catalysts Synthesized in Situ from Bimetallic Precursors Dissolved in Acetone for the Heavy Oil Upgrading, *J. Anal. Appl. Pyrolysis*, 2025, 107454.

13 Y. Zhou, Q. Zhao, Z. Song, J. Wang, Y. Zhang and L. Guo, Kinetic Study on Catalysis and Coordination Bonding of Cu Atoms in the Heavy Oil Aquathermolysis Catalyzed by $CuSO_4$ and $CuSO_4$/NaOH, *Energy Fuels*, 2025, **39**, 15435–15446.

14 P. Schacht-Hernández, J. L. García-Gutiérrez, R. Quintana-Solórzano, F. Jiménez-Cruz and A. D. Miranda-Olvera, In Situ Heavy Crude Oil Upgrading via Catalytic Aquathermolysis with a Nickel-Based Catalyst Deposited Over a Rock Matrix, *ACS Omega*, 2026, **11**(1), 773–783.

15 E. A. Jaseer, A. Musa, B. M. Al Otaibi, M. R. Aldossary, A. Tanimu, N. Maity, S. Barman, S. A. Al-Jendan and A. Aitani, Homogeneous Catalysis in Aquathermolysis for Heavy Oil Upgrading: A Critical Review of Advances, Challenges, and Perspectives, *Energy Fuels*, 2025, **39**(17), 7941–7966.

16 S. Li, J. Tuo, Z. Wan, S. Zhang, M. Yu, Y. Ma, R. Peng, H. Xu, J. Jiang, S. Chen, X. He and P. Wu, Controllable Synthesis of Hollow Mesoporous ZSM-5 with Improved Catalytic Performance for Tetralin Hydrocracking to Light Aromatics, *Ind. Eng. Chem. Res.*, 2025, **64**(8), 4330–4341.

17 P. Sun, X. Fang, Y. Du, Y. Li and C. Peng, Study on the Preparation and Structural Properties of Core–Shell Hierarchical Pore Molecular Sieve Synthesized by a Silicon Coating Method, *Ind. Eng. Chem. Res.*, 2024, **63**(48), 20747–20755.

18 S. Rudyk, Relationships between SARA Fractions of Conventional Oil, Heavy Oil, Natural Bitumen and Residues, *Fuel*, 2018, **216**, 330–340.

19 R. Abolivier, E. Hans-Georg and J. A. Sullivan, Study of Ni-ZSM-5 Catalysts in the Hydrogenolysis of Benzyl Phenyl Ether: Effects of Ni Loading, Morphology, and Reaction Conditions, *ACS Omega*, 2025, **10**(12), 12306–12318.

20 K. Tian, W. Pu, Q. Wang, M. Xie, S. Liu and X. Zhu, Study on the Influence of SARA Fraction in Heavy Oil on the Oil Recovery During Water Flooding by Experiments and the Molecular Dynamics Simulation, *J. Dispersion Sci. Technol.*, 2025, **46**(7), 1127–1138.

21 H. B. Gao, Y. L. Wang, X. Yan, H. J. Liu, W. H. Zhao, W. J. Gu and Y. P. Zhao, Construction of b-Axis-Oriented ZSM-5 Nanosheets for Improved Catalytic Upgrading of Lignite Pyrolysis Volatiles to Light Aromatic Hydrocarbons: Synergy and Balance between Acidity and Diffusivity, *Energy Fuels*, 2025, **39**(21), 9981–9996.

22 K. Saenluang, T. Imyen, W. Wannapakdee, D. Suttipat, P. Dugkhuntod, M. Ketkaew and C. Wattanakit, Hierarchical Nanospherical ZSM-5 Nanosheets with Uniform Al Distribution for Alkylation of Benzene with Ethanol, *ACS Appl. Nano Mater.*, 2020, **3**(4), 3252–3263.

23 A. Tirado, G. Félix, A. A. Al-Muntaser, M. A. Suwaid, M. A. Varfolomeev and J. Ancheyta, Kinetics of Non-Catalytic Aquathermolysis of Heavy Crude Oil in the

Presence of a Hydrogen Donor, *Ind. Eng. Chem. Res.*, 2024, **63**(19), 8601–8609.

24 Z. Pang, Q. Wang, C. Tian and J. Chen, Study on Hydrothermal Cracking of Heavy Oil under the Coexisting Conditions of Supercritical Water and Non-condensate Gas, *ACS Omega*, 2023, **8**(20), 18029–18040.

25 L. Qin, J. Li, S. Zhang, Z. Liu, S. Li and L. Luo, Catalytic Performance of Ni–Co/HZSM-5 Catalysts for Aromatic Compound Promotion in Simulated Bio-oil Upgrading, *RSC Adv.*, 2023, **13**, 7694–7702.

26 F. Coumans, B. Mezari, N. Zuidema, J. M. J. J. Heinrichs and E. J. M. Hensen, Isolating Al Surface Sites in Amorphous Silica–Alumina by Homogeneous Deposition of Al^{3+} on SiO_2 Nanoparticles, *ACS Appl. Nano Mater.*, 2024, **7**, 25524–25534.

27 S. Tsubota, S. Kokuryo, K. Miyake, Y. Uchida, A. Mizusawa, T. Kubo and N. Nishiyama, Understanding the Role of the Surface Acidity of MFI Zeolites during LDPE Cracking: Decomposition Temperature and Product Distribution, *ACS Catal.*, 2024, **14**, 18145–18155.

28 Q. Wang, S. Zhang, X. Chen, J. Ni, J. Du, Y. Li, X. Xin, B. Zhao and G. Chen, Synergistic Catalysis of Water-Soluble Exogenous Catalysts and Reservoir Minerals during the Aquathermolysis of Heavy Oil, *Molecules*, 2024, **29**, 3761.

29 Z. Yang, Y. Liu, J. Jiang, L. Pan, D. Wei, X. Feng, L. He, J. Guo and Y. Zhang, A Multi-Component and Multi-Functional Synergistic System for Efficient Viscosity Reduction of Extra-Heavy Oil, *Molecules*, 2025, **30**, 4446.

30 A. N. Khamieva, A. A. Al-Muntaser, M. A. Suwaid, R. Djimasbe, S. U. Reyimkulyyeva, D. A. Emelianov and M. A. Varfolomeev, Synthesis and Application of a Ni-Based Dispersed Catalyst for Hydrothermal Upgrading of Heavy Crude Oil, *Energy Fuels*, 2024, **38**, 1204–1215.

31 Y. I. I. Abdelsalam, L. K. Galiakhmetova, A. V. Sharifullin, A. Tajik, R. E. Mukhamatdinova, R. R. Davletshin and A. V. Vakhin, Comparative Study of the Catalytic Effects of $Al(CH_3COO)_3$ and $Al_2(SO_4)_3$ on Heavy Oil Aquathermolysis in CO_2 and N_2 Atmospheres, *Appl. Catal., A*, 2025, **699**, 120247.

32 J. Hu, J. Yang, P. Wang, X. Gu and G. Chen, Improvement of the Fluidity of Heavy Oil Using a Composite Viscosity Reducer, *Processes*, 2025, **13**, 3547.

33 T. Kahs, J. Whelan, Z. Alhaddad, M. Witt, E. Larkin, S. Punnapala, D. Abdallah and P. Naumov, Molecular Composition of Middle Eastern Asphaltenes by Mass Spectrometry: Field vs Dead-Oil-Derived Deposits, *Energy Fuels*, 2024, **38**(21), 20324–20336.

34 G. Félix, A. Tirado, M. A. Varfolomeev and J. Ancheyta, Effect of Reaction Pathways on the Kinetic Modeling of Aquathermolysis of Heavy Oils, *Ind. Eng. Chem. Res.*, 2024, **63**(42), 17836–17846.

35 A. Tirado, G. Félix, M. A. Suwaid, A. A. Al-Muntaser, M. A. Varfolomeev and J. Ancheyta, A Comparative Analysis of Aquathermolysis Kinetics in Heavy Oils: Benchmarking Reaction Pathways across Multiple Systems, *Ind. Eng. Chem. Res.*, 2025, **64**(33), 16091–16100.

36 A. Tirado, G. Félix, M. A. Varfolomeev and J. Ancheyta, Kinetic Analysis of Asphaltene Conversion under Supercritical Water Conditions, *Ind. Eng. Chem. Res.*, 2024, **63**(26), 11334–11343.

37 Z. Fu, The Use of Metal/ZSM-5 Nanosheet for Efficient Catalytic Cracking of Cross-Linked Polyethylene for High-Voltage Cable Insulation, *Materials*, 2025, **18**, 4675.

38 L. B. Krivdin, Liquid-Phase NMR of Asphaltenes, *Magn. Reson. Chem.*, 2024, **62**, 670–685.

39 A. N. Zargar, A. Kumar, A. Sinha, M. Kumar, I. Skiadas, S. Mishra and P. Srivastava, Asphaltene Biotransformation for Heavy Oil Upgradation, *AMB Express*, 2021, **11**, 127.

40 Y. Ma, W. Deng, G. Li, S. Ullah, Z. Zhang, L. Chen and X. Zhou, Structural and Electrochemical Enhancement of FCC Slurry Oil-Derived Pitch via Asphaltene-Driven Graphitic Ordering, *ACS Omega*, 2025, **10**, 21823–21834.

41 S. K. Maity, J. Ancheyta and G. Marroquín, Catalytic Aquathermolysis Used for Viscosity Reduction of Heavy Crude Oils: A Review, *Energy Fuels*, 2010, **24**, 2809–2816.

42 T. Kholmurodov, O. Mirzaev, B. Affane, A. Tajik, K. Romanova, Y. Galyametdinov, A. Dengaev and A. Vakhin, Thermochemical Upgrading of Heavy Crude Oil in Reservoir Conditions, *Processes*, 2023, **11**, 2156.

43 V. Katnov, M. A. Khelkhal, S. Trubitsina, I. Kiselev, L. Galiakhmetova, E. Usmanova, N. Nazimov and A. Vakhin, In-situ upgrading of heavy oil via aquathermolysis using metallic sodium nanosuspension: Thermal treatment optimization and mechanistic investigation, *Fuel*, 2026, **404**, 136344.